Pergamon

Int. J. Heat Mass Transfer. Vol. 38, No. 2, pp. 189–205, 1995

0017–9310/95 $9.50+0.00

0017–9310(94)00212–6

Modelling the temperature profiles within boards during the high-temperature drying of *Pinus radiata* timber: the influence of airflow reversals

PANG SHUSHENG and R. B. KEEY

Department of Chemical and Process Engineering, University of Canterbury, Private Bag 4800, Christchurch, New Zealand

and

T. A. G. LANGRISH†

Department of Chemical Engineering, University of Sydney, N.S.W. 2006, Australia

(*Received for publication in final form* 29 *July* 1994)

Abstract—Profiles of the surface and centre temperatures in the high-temperature drying of *Pinus radiata* have been predicted as a function of time for heartwood and sapwood boards, using a receding evaporative plane model, which incorporates equations for local heat and mass balances, internal and external heat transfer, and internal moisture fluxes due to bound-water diffusion and flow of water vapour and liquid water. The model predictions have been compared with independent measurements of the temperatures at the surface and centre of sapwood, heartwood and mixed-wood boards. The simulated and measured temperature profiles are in good agreement except that the outer temperatures are predicted to rise more swiftly when the evaporative plane starts to recede in the wood, while the inner temperatures are estimated to rise more sluggishly once the first period is over. However, the maximum discrepancies in these three cases are less than 6°C, and may be due to difficulties in getting accurate measurements of local temperatures when these are changing. This model is used to predict local temperature and moisture-content profiles in high-temperature kiln drying of this timber for conditions with airflow reversals. Variations have been reported in the external mass-transfer coefficients in the streamwise direction which lead to differential drying of the boards. The differences in the extent of drying across each board can be reduced by reversing the airflow periodically. Airflow reversals every 4 h are adequate to give a high degree of uniformity in the final temperature and moisture-content profiles for heartwood after 24 h of drying, and may be sufficient for sapwood if a small degree of variation is acceptable. Flow reversals every 8 h yield essentially the same result.

INTRODUCTION

High-temperature drying, involving the use of dry-bulb temperatures greater than 100°C, is rapidly becoming the preferred commercial practice in New Zealand for drying softwood plantation timber, such as *Pinus radiata*. Tests at the Forest Research Institute, Rotorua [1], indicate that internal temperatures can remain at the boiling point for some time during the drying process for heartwood. The calculations of Stanish and his colleagues [2] for a North American softwood, southern pine, also show this feature, although the authors did not specifically comment on the phenomenon. The appearance of such a temperature plateau has led us to propose a model of drying based upon a receding evaporative front until the timber reaches the fibre-saturation point.

Softwoods such as *P. radiata* have a relatively simple anatomy of long, pointed cells called tracheids providing both structural support and conducting pathways for the tree. Wood is produced by a thin zone of cells near the outside of the trunk or branch just beneath the bark. The outer portion of the stem is sapwood which is active in the transport of water and nutrients. When trees of *P. radiata* are about 15 years old, heartwood is formed, spreading upwards and outwards with age in a cone within the trunk. The cells are dead within the heartwood, which is characterized by an accumulation of polyphenolic resins and a reduction in moisture content. The bordered pits in sapwood, when open or unaspirated, allow fluid to pass between tracheids. When these pits are closed or aspirated, this movement is no longer possible and the permeability to moisture is reduced markedly. Pit aspiration occurs in the formation of heartwood, possibly due to the formation of resins, and when the tree is felled as a physiological response to heal the damage. A comparison of property values

† Author to whom correspondence should be addressed.

NOMENCLATURE

a coefficient in equation (20)
A constant in equation (11) [Pa]
b coefficient in equation (20)
B constant in equation (11)
c coefficient in equation (25)
C_P specific heat capacity of moist wood [J kg^{-1} K^{-1}]
C_{PG} specific heat capacity of dry gas [J kg^{-1} K^{-1}]
C_{PV} specific heat capacity of vapour [J kg^{-1} K^{-1}]
C_{PY} humid heat capacity [J kg^{-1} K^{-1}]
d coefficient in equation (25)
D apparent moisture-diffusion coefficient, equation (16) [kg m^{-1} s^{-1}]
D_b bound-water diffusion coefficient [kg s m^{-3}]
E_l effective permeability to liquid flow [s]
E_V effective permeability to vapour flow [s]
F external mass-transfer coefficient based on molar concentration differences [mol m^{-2} s^{-1}]
h heat-transfer coefficient [W m^{-2} K^{-1}]
ΔH_{vb} latent heat of vaporization of bound water [J kg^{-1}]
ΔH_{vw} latent heat of vaporization of liquid water [J kg^{-1}]
j_{tot} total vapour flux from the surface [kg m^{-2} s^{-1}]
j_{wb} flux of bound water [kg m^{-2} s^{-1}]
j_{wf} liquid water flux [kg m^{-2} s^{-1}]
$j_{wf\xi}$ liquid water flux just beneath the evaporative plane [kg m^{-2} s^{-1}]
j_{wv} water vapour flux [kg m^{-2} s^{-1}]
$j_{wv\xi}$ water vapour flux just beneath the evaporative plane [kg m^{-2} s^{-1}]
K_l permeability of unsaturated wood to liquid movement [m^2]
K_l^s permeability of saturated wood to liquid movement [m^2]
K_G permeability of wood to the movement of water vapour [m^2]
K_Y external mass-transfer coefficient based on mass concentration differences [kg m^{-2} s^{-1}]
m_G molar mass of air [kg mol^{-1}]
m_v molar mass of water vapour [kg mol^{-1}]
p_c capillary pressure [Pa]
p_l liquid pressure [Pa]
$\overline{p^G}$ average partial pressure of air in the airstream [Pa]
p_t total pressure of the airstream [Pa]
p^V moisture vapour pressure [Pa]
p_G^V bulk-gas value of the moisture vapour pressure [Pa]
p_s^V partial pressure of moisture vapour at the board surface [Pa]
q source term in equation (25)
r source term in equation (20)
s entropy [J mol^{-1} K^{-1}]
S saturation
S_{min} minimum saturation for liquid flow
T temperature [K]
T_G gas temperature [K]
T_j temperature at node j [K]
v molar volume [m^3 mol^{-1}]
x distance from the leading edge of a board [m]
X local moisture content, dry basis [kg kg^{-1}]
$\bar{X}$ local average moisture content, dry basis [kg kg^{-1}]
X_ξ moisture content just below the evaporative plane [kg kg^{-1}]
X_{FSP} moisture content at the fibre saturation point [kg kg^{-1}]
X_j moisture content at node j [kg kg^{-1}]
X_{max} moisture content if the entire void structure were filled with water [kg kg^{-1}]
X_{min} minimum moisture content for liquid flow [kg kg^{-1}]
$\langle X_N \rangle$ average moisture content in the region between nodes N and $N+1$ [kg kg^{-1}]
X_o initial moisture content [kg kg^{-1}]
Y_G gas humidity, dry basis [kg kg^{-1}]
z space coordinate measured normal to the surface [m]
Δz size of distance increment [m].

Greek symbols
β external mass-transfer coefficient based on partial-pressure differences [s m^{-1}]
δ half-thickness of the board [m]
ε void fraction
η_G viscosity of water vapour [kg m^{-1} s^{-1}]
η_l viscosity of water [kg m^{-1} s^{-1}]
λ thermal conductivity of moist wood [W m^{-1} K^{-1}]
μ_b chemical potential for bound water [J kg^{-1}]
μ_v chemical potential for water vapour [J kg^{-1}]
ξ dry-layer thickness [m]
$\Delta\xi$ distance of evaporative plane movement [m]
ξ_o initial distance of the evaporative plane from the surface for sapwood [m]
ρ_G density of water vapour [kg m^{-3}]
ρ_l density of water [kg m^{-3}]

ρ_s	density of dry wood [kg m^{-3}]	Subscript	
τ	time [s]	j	node point.
$\Delta\tau$	time interval [s]		
ξ	distance of the evaporative plane from the surface [m]	Superscripts	
		n	current time step
ξ_o	initial thickness of the thin dry layer near the surface [m]	o	previous time step.
$\Delta\xi$	change in position of evaporative plane [m].		

between sapwood and heartwood is shown in Table 1, highlighting the differences in initial moisture content, basic density and vapour permeability which arise from the differences in structure.

Previous studies of timber drying [2, 3] have only considered the effect of air flowing in one direction. However, in practical kiln operation, the airflow is reversed periodically to achieve more uniform drying. In this investigation, we describe the transfer processes, the phase equilibria and the method of solution before comparing the predictions with experimentally-measured temperature profiles. Then we predict the local temperature and moisture-content profiles along a board for both unidirectional airflow and airflow reversals using our drying model and the mass-transfer data reported by Kho *et al.* [4]. These predictions indicate the benefits of airflow reversals for sapwood and heartwood in terms of improved moisture uniformity within boards, and suggest the number of airflow reversals beyond which little further benefit can be expected.

The physical process of drying for P. radiata

The properties of softwood timber vary substantially from sapwood to heartwood. The bordered pits in the cell wall between vessels generally aspirate when coniferous trees such as *P. radiata* form heartwood. This process significantly retards the liquid flow within the timber. However, the pits in sapwood are usually not aspirated when the sapwood is green, since the pits are required for the transport of liquid material. They aspirate only when the sapwood is dried, and this aspiration process is irreversible [5].

This difference is relevant to the drying of timber because the degree of pit aspiration governs the permeability of the timber to the flow of liquid. The permeability of the timber to liquid flow becomes very low once the pits are aspirated and the pits are blocked.

Table 1. A comparison between the properties of *P. radiata* sapwood and heartwood

	Sapwood	Heartwood
Initial moisture content [kg kg^{-1}] [12]	1–2	0.4–0.5
Basic density [kg m^{-3}] [12]	430–505	338–404
Vapour permeability [10^{-15} m^2] [11]	32–138	8.8–78.6

We have divided the process of high-temperature drying of *P. radiata* heartwood into an initial drying period and a second one. During the initial period, it is postulated that there exists an evaporative plane at which all the free water evaporates. Since the liquid flow is insignificant beneath the plane due to the pit aspiration, this plane will recede into the material as drying proceeds. The evaporative plane divides the material into two parts, a wet zone beneath the plane and a dry zone above it. Above the plane, moisture is assumed to exist as bound water and water vapour. Bound water will be in local thermodynamic equilibrium with the vapour pressure of water at the local temperature [3]. In the wet zone, the moisture content remains at the initial value.

After the evaporative plane reaches the centre-layer of the board, drying is controlled by bound-water diffusion and water vapour flow. We will call this the second drying period.

In the drying of sapwood boards, the flow of liquid moisture close to the surface is insignificant because most of the pits near the surface are aspirated during storage after the wood has been sawn. Therefore, at the beginning of the initial drying period of sapwood, the evaporative plane recedes into the material very quickly. However, when the plane reaches a certain distance ξ_o from the surface, most of the pits inside this position are not yet aspirated and the flow of liquid is no longer negligible. The liquid flow towards the surface will keep the evaporative plane at the position ξ_o until the moisture content at the plane decreases to the minimum value for liquid continuity. After this, the plane starts to recede into the material. The main difference between the drying behaviour of sapwood and heartwood during this initial period is that the liquid flow in the wet zone for sapwood has a significant influence on the receding velocity of the evaporative plane. Thereafter, the drying process for sapwood is similar to that for heartwood.

There is some evidence for the appearance of an evaporative zone close to the exposed surface. Kiln operators note the appearance of a 'brown stain', believed to be from resinous deposits, at a depth of 0.5–1 mm below the surface. This is of similar order

to the values of ξ_o which we use in this work: 0.3 mm (sapwood); 0.45 mm (mixed wood).

THE EQUATIONS FOR THE TEMPERATURE AND MOISTURE-CONTENT PROFILES

The heat- and mass-conservation equations in the dry zone during the first period and within the whole material during the second period are as follows:

$$C_P \cdot \rho_s \cdot \frac{\partial T}{\partial \tau} = \frac{\partial}{\partial z}\left(\lambda \cdot \frac{\partial T}{\partial z}\right) - \Delta H_{vb} \cdot \frac{\partial j_{wv}}{\partial z} \quad (1)$$

and

$$-\rho_s \cdot \frac{\partial X}{\partial \tau} = \frac{\partial}{\partial z} \cdot (j_{wv} + j_{wb}) \quad (2)$$

where C_p is the specific heat capacity of moist wood, X is the local moisture content in the wood, ρ_s is the density of dry wood, T is the temperature, τ is the time, z is the space coordinate measured normal to the surface of the board, λ is the thermal conductivity of the moist wood, j_{wv} is the water vapour flux, j_{wb} is the flux of bound water, and ΔH_{vb} is the latent heat of vaporization of bound water.

If the flux of water vapour is assumed to be proportional to the gradient of the vapour partial pressure, then the vapour flux in the dry zone is given by

$$j_{wv} = -E_V \cdot \frac{\partial p^V}{\partial z} \quad (3)$$

where E_V is the effective permeability to vapour flow, and p^V is the vapour partial pressure.

The effective permeability to vapour flow (E_V) may be related to the commonly measured permeability (K_G) by the equation

$$E_V = \frac{K_G \cdot \rho_G}{\eta_G} \quad (4)$$

where ρ_G and η_G are the density and viscosity of the vapour, respectively.

The vapour partial pressure can be calculated as a function of local temperature and moisture content using the relationship given by Simpson and Rosen [6] with some correction for the particular species of wood, *P. radiata*.

If we use the chemical potential (μ) as the driving force for the movement of bound water, then the flux of bound water is given by the equation

$$j_{wb} = -D_b \cdot (1-\varepsilon) \cdot \frac{d\mu_b}{dz} \quad (5)$$

where D_b is the bound-water transfer coefficient, ε is the void fraction of the timber, and the subscript b refers to bound water. Further, there is local thermodynamic equilibrium between the bound water and the vapour, so the chemical potential of the bound water (μ_b) is equal to that of the vapour (μ_v) and it follows that

$$m_v \cdot d\mu_b = m_v \cdot d\mu_v = -s \cdot dT + v \cdot dp^v \quad (6)$$

where m_v is the molar weight of water, and v is the molar volume of water vapour. The molar entropy s is a state function of temperature and pressure. Stanish *et al.* [2] show that equations (5) and (6) reduce to the working expression

$$j_{wb} = -\frac{D_b \cdot (1-\varepsilon)}{m_v}\left\{-\left[187 + 35.1 \cdot \ln\left(\frac{T}{298.15}\right)\right.\right.$$
$$\left.\left. - 8.314 \cdot \ln\left(\frac{p^V}{101\,325}\right)\right] \cdot \frac{\partial T}{\partial z} + 8.314 \cdot \frac{T}{p^V} \cdot \frac{\partial p^V}{\partial z}\right\}. \quad (7)$$

In the wet zone, there are no significant vapour flows, so the fluxes j_{wv} and j_{wb} are zero in this region. Also, there is no liquid flow in this zone within heartwood, and the moisture content below the evaporative plane is everywhere equal to the initial moisture content.

For sapwood, however, the moisture content is initially high, so, when water evaporates at the evaporative plane, unbound water beneath the plane will flow towards it due to capillary forces. This process can be described by Darcy's law. The pressure gradient is assumed to be a consequence of the capillary action between the liquid and gas phases within the voids of the wood. Thus, we obtain the liquid water flux within the wood (j_{wf}) as

$$j_{wf} = -E_l \cdot \frac{\partial p_l}{\partial z} = E_l \cdot \frac{\partial p_c}{\partial z} \quad (8)$$

where p_l is the liquid pressure, p_c is the capillary pressure, and E_l is the effective permeability to liquid flow.

The effective permeability (E_l) can also be related to the commonly measured permeability (K_l) by the equation

$$E_l = \frac{K_l \cdot \rho_l}{\eta_l} \quad (9)$$

where ρ_l and η_l are the density and viscosity of the liquid water, respectively, and K_l is the permeability to liquid flow. Both the capillary pressure (p_c) and the liquid permeability (K_l) are functions of the saturation (S), defined by

$$S = \frac{\text{liquid volume}}{\text{void volume}} = \frac{X - X_{FSP}}{X_{max} - X_{FSP}} \quad (10)$$

where X_{FSP} is the moisture content at the fibre-saturation point when the voids are empty, and X_{max} is the moisture content of the wood if the entire void structure were filled with liquid.

For softwood, Spolek and Plumb [7] assume that the capillary pressure is a simple function of saturation

$$p_c = A \cdot S^{-B} \quad (11)$$

where A and B are constants. Stanish *et al.* [2] correlate the permeability (K_l) of the unsaturated wood with that measured at saturation (K_l^s) by the expression

$$K_l = K_l^s \cdot \left\{1.0 - \cos\left[\frac{\pi}{2} \cdot \left(\frac{S - S_{min}}{1.0 - S_{min}}\right)\right]\right\}. \quad (12)$$

The minimum saturation for liquid flow within the board is S_{min}.

From equations (8), (10) and (11), the relationship between the liquid water flux and the local moisture content becomes

$$j_{wf} = -\frac{A \cdot B \cdot E_l \cdot (X_{max} - X_{FSP})^B}{(X - X_{FSP})^{(1+B)}} \cdot \frac{\partial X}{\partial z}. \quad (13)$$

The equation for moisture conservation enables the change in moisture content with time to be related to the gradient of this flux as follows:

$$\rho_s \cdot \frac{\partial X}{\partial \tau} = -\frac{\partial j_{wf}}{\partial z}. \quad (14)$$

The equation for the movement of liquid water in the wet zone has a similar form to that for heat conduction [equation (2)]. By combining equations (13) and (14) we obtain

$$\rho_s \cdot \frac{\partial X}{\partial \tau} = \frac{\partial}{\partial z}\left(D \cdot \frac{\partial X}{\partial z}\right) \quad (15)$$

where the apparent moisture-diffusion coefficient (D) is given by

$$D = \frac{A \cdot B \cdot E_l \cdot (X_{max} - X_{FSP})^B}{(X - X_{FSP})^{(1+B)}}. \quad (16)$$

The external mass-transfer coefficient (β) affects the boundary condition at the surface of the boards, and the total vapour flux from the surface (j_{tot}) is given by

$$j_{tot} = -\frac{d}{dt}[\bar{X} \cdot \rho_s \cdot l] = \beta \cdot (p_s^V - p_G^V) \quad (17)$$

where $\bar{X}$ is the local average moisture content, l is the half-layer thickness (just below the surface), p_s^V is the partial pressure of moisture vapour at the board surface, and p_G^V is the bulk-gas value of the moisture vapour pressure.

The velocity of the receding evaporative plane has been predicted from the local moisture mass balance around the plane. If the evaporative plane recedes a distance $\Delta\xi$ during a time interval $\Delta\tau$, the moisture loss in this region should be equal to the time interval multiplied by the flux difference between the vapour just above the plane ($j_{wv\xi}$) and the liquid water just beneath it ($j_{wf\xi}$). That is:

$$\Delta\xi \cdot \rho_s \cdot (X_\xi - X_{FSP}) = -(j_{wv\xi} - j_{wf\xi}) \cdot \Delta\tau \quad (18)$$

where X_ξ is the moisture content just beneath the plane.

We can use equations (1)–(18) to predict the temperature (T) and the moisture content (X) in both the dry and wet zones, the bound-water flux (j_{wb}) and the water vapour flux (j_{wv}) in the dry zone, and the liquid-water flux in the wet zone (j_{wf}) for sapwood. We can solve the model numerically if the initial and boundary conditions and the various transport coefficients are known, and the method adopted will be described in the next section.

SOLVING THE HEAT- AND MASS-TRANSFER EQUATIONS USING A NUMERICAL METHOD

We will solve the equations in the model in the following order. First, the heat conservation equation (1) will be solved for the temperature profiles within the timber. This enables the water vapour flux [j_{wv}, equation (3)] and the bound-water flux [j_{wb}, equation (7)] to be calculated in the dry zone, so the mass conservation equation (2) may be solved in the dry zone. For sapwood, the moisture content in the wet zone may be estimated from equations (15) and (16). These equations are non-linear and interlinked. For example, the water vapour flux appears in the heat conservation equation. Therefore, the above procedure was repeated until all the temperatures changed from iteration to iteration by less than 0.001 K.

Solving the heat-conservation equation for the temperature profiles

The general form of equation (1) is

$$C_P \cdot \rho_s \cdot \frac{\partial T}{\partial \tau} = \frac{\partial}{\partial z}\left(\lambda \cdot \frac{\partial T}{\partial z}\right) + \Phi \quad (19)$$

where Φ is a source term involving the latent heat of vaporization. The Ackermann correction factor for heat transfer is negligible at the mass-transfer rates in the kiln. In the dry zone during the first period, and within the whole material during the second period,

$$\Phi = -\Delta H_{vb} \cdot \frac{\partial j_{wv}}{\partial z}.$$

In the wet zone, $\Phi = 0$, while at the evaporative plane

$$\Phi = \Delta H_{vw} \cdot \frac{j_{wv\xi}}{(\Delta z - \Delta z_\xi)}$$

where ΔH_{vw} is the latent heat of vaporization of liquid water, $j_{wv\xi}$ is the vapour flux just above the evaporative plane, and $(\Delta z - \Delta z_\xi)$ is the distance to the node just beneath it when the temperature is calculated (Fig. 2).

The board is divided into $2J$ uniformly spaced nodes, as shown in Fig. 1. The temperature at a node j at the nth iteration is obtained from those at the

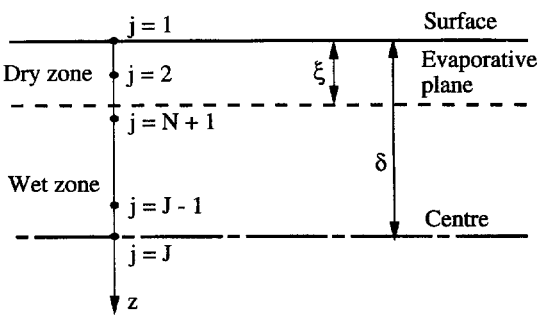

Fig. 1. The grid points over a half-width of the board.

adjacent nodes by a fully implicit discretization of equation (19) [8]. The result is

$$b_j \cdot T_j^n = a_{j+1} \cdot T_{j+1}^n + a_{j-1} \cdot T_{j-1}^n + r_j \qquad (20)$$

for $j = 2, \ldots, J-1$.

The various coefficients in the equation are given by

$$a_{j+1} = \frac{\lambda_{j+1}}{(\Delta z)_{j+1}} \quad a_{j-1} = \frac{\lambda_{j-1}}{(\Delta z)_{j-1}}$$

$$a_j^o = \left(\frac{\rho_s \cdot C_P \cdot \Delta z}{\Delta \tau}\right)_j \quad b_j = a_{j-1} + a_{j+1} + a_j^o$$

which Δz is the size of the distance increment, and $\Delta \tau$ is the size of the time step. The source term in equation (20) becomes

$$r_j = a_j^o \cdot T_j^o + \Phi_j \cdot \Delta z$$

where the superscript o on the temperature is the temperature from the previous time step. Rearranging equation (20), it follows that

$$-a_{j-1} \cdot T_{j-1}^n + b_j \cdot T_j^n - a_{j+1} \cdot T_{j+1}^n = r_j. \qquad (21)$$

Boundary conditions are required in order to obtain the full solution of equation (21).

From the heat balance at the surface of the board, the heat-transfer equation becomes

$$b_1 \cdot T_1^n - a_2 \cdot T_2^n = r_1 \qquad (22)$$

with

$$r_1 = h \cdot T_G + a_1^o \cdot T_1^o + \Phi_1 \cdot \Delta z,$$

and

$$b_1 = a_2 + a_1^o + h,$$

where h is the heat-transfer coefficient to the board surface and T_G is the bulk gas temperature.

At the centre of the board, since the temperature profile is symmetrical about the mid-layer, we know that

$$T_{J+1}^n = T_{J-1}^n \quad a_{J+1} = a_{J-1}.$$

Therefore the heat-transfer equation at the centre of the board becomes

$$-2 \cdot a_{J-1} \cdot T_{J-1}^n + b_J \cdot T_J^n = r_J. \qquad (23)$$

All the heat-transfer equations at any point in time may be represented in matrix notation as

$$\begin{bmatrix} b_1 & -a_2 & 0 & 0 & \ldots & 0 \\ -a_1 & b_2 & -a_3 & 0 & \ldots & 0 \\ \vdots & \vdots & \vdots & \vdots & \vdots & \vdots \\ 0 & \ldots & 0 & -a_{J-2} & b_{J-1} & -a_J \\ 0 & \ldots & 0 & 0 & -2 \cdot a_{J-1} & b_J \end{bmatrix} \cdot \begin{bmatrix} T_1 \\ T_2 \\ \vdots \\ T_{J-1} \\ T_J \end{bmatrix} = \begin{bmatrix} r_1 \\ r_2 \\ \vdots \\ r_{J-1} \\ r_J \end{bmatrix}. \qquad (24)$$

This tridiagonal system of equations was solved using a subroutine from Press *et al.* [9].

Solving the mass-conservation equation for the moisture content in the wet zone

Again, we use a fully implicit discretization of equation (15) using the technique described by Patankar [8]. The result is

$$d_j \cdot X_j^n = c_{j+1} \cdot X_{j+1}^n + c_{j-1} \cdot X_{j-1}^n + q_j \qquad (25)$$

for $j = N+2, \ldots, J-1$.

The various coefficients are given by

$$c_{j+1} = \frac{D_{j+1}}{(\Delta z)_{j+1}} \quad c_{j-1} = \frac{D_{j-1}}{(\Delta z)_{j-1}}$$

$$c_j^o = \left(\frac{\rho_s \cdot \Delta z}{\Delta \tau}\right)_j \quad d_j = c_{j-1} + c_{j+1} + c_j^o$$

and the source term becomes

$$q_j = c_j^o \cdot X_j^o.$$

Boundary conditions are needed to give the full solution of equation (25) for all nodes in the wet zone.

The moisture-transfer equation for the two nodes just beneath the evaporative plane and the point at the plane becomes

$$-c_\xi \cdot X_\xi^n + c_{N+1} \cdot X_{N+1}^n - c_{N+2} \cdot X_{N+2}^n = q_{N+1} \qquad (26)$$

where

$$c_\xi = \frac{D_\xi}{(\Delta z)_\xi}.$$

At the centre of the board, the moisture-content profile is symmetrical about the mid-layer, so we can write a similar equation to equation (23) for heat transfer, as follows:

$$-2 \cdot c_{J-1} \cdot X_{J-1}^n + d_J \cdot X_J^n = q_J. \qquad (27)$$

Equations (25)–(27) may be rearranged in matrix notation as

$$\begin{bmatrix} d_{N+1} & -c_{N+2} & 0 & 0 & \ldots & 0 \\ -c_{N+1} & d_{N+2} & -c_{N+3} & 0 & \ldots & 0 \\ \vdots & \vdots & \vdots & \vdots & \vdots & \vdots \\ 0 & \ldots & 0 & -c_{J-2} & d_{J-1} & -c_J \\ 0 & \ldots & 0 & 0 & -2 \cdot c_{J-1} & d_J \end{bmatrix} \cdot \begin{bmatrix} X_{N+1} \\ X_{N+2} \\ \vdots \\ X_{J-1} \\ X_J \end{bmatrix} = \begin{bmatrix} q_{N+1} \\ q_{N+2} \\ \vdots \\ q_{J-1} \\ q_J \end{bmatrix}. \qquad (28)$$

At first, the moisture content (X_ξ) at the evaporative plane will be greater than the minimum value (X_{min}) for liquid continuity. Before the plane begins to recede, the moisture contents at the plane will decrease and the moisture contents in the wet zone will change

correspondingly. However, an equation to relate explicitly the moisture content just beneath the plane to that just above it (the fibre-saturation point) cannot be stated, so we have to adjust the moisture content just below the plane to satisfy mass conservation within the whole wet zone. Here, the total moisture loss from the wet zone during a time interval $\Delta\tau$ should equal the liquid flux just beneath the evaporative plane $[(j_{wf})_{\xi}+]$ multiplied by this time interval. This gives

$$\left[\sum_{N+2}^{J-1}\Delta z\cdot(X_j^n-X_j^o)\cdot\rho_s\right]+0.5\cdot\Delta z\cdot\rho_s\cdot[(X_{N+1}^n-X_{N+1}^o)+(X_j^n-X_j^o)]-\Delta\tau\cdot(j_{wf})_{\xi}+=0. \quad (29)$$

In solving this equation, the secant method is applied at each time step. Once the moisture content at the evaporative plane has decreased to the minimum value for liquid continuity (X_{min}), it will remain constant and equal to X_{min}.

The moisture content just above the evaporative plane

The moisture content at the node just beneath the evaporative plane may be estimated from a local mass balance in the vicinity of the evaporative plane (Fig. 2). At the evaporative plane, we postulate a moisture content jump between the wet-side value, $X_{\xi}=X_{min}$, and the dry-side value (X_{FSP}) at fibre saturation. This contrivance is an approximation to what we believe to be the actual profile: a very rapid transition over perhaps one tracheid width.

For the area between nodes N and $N+1$, the mass balance equation is

$$\langle X_N\rangle\cdot\Delta z=(\Delta z-\Delta z_{\xi})\cdot\frac{(X_{\xi}+X_{N+1})}{2}+\Delta z_{\xi}\cdot\frac{(X_{FSP}+X_N)}{2} \quad (30)$$

where $\langle X_N\rangle$ is the average moisture content in the region between the node $N+1$ just beneath the evaporative plane and the node N just above it. The variables $\langle X_N\rangle$, Δz_{ξ} and X_N will vary with time, so equation (30) may be differentiated to give

$$\Delta z\cdot\frac{\partial\langle X_N\rangle}{\partial\tau}=0.5\cdot(X_{FSP}+X_N-X_{N-1}-X_{\xi})\cdot\frac{\partial\xi}{\partial\tau}+0.5\cdot(\Delta z-\Delta z_{\xi})\cdot\left(\frac{\partial X_{N+1}}{\partial\tau}+\frac{\partial X_{\xi}}{\partial\tau}\right)+0.5\cdot\Delta z_{\xi}\cdot\frac{\partial X_N}{\partial\tau}. \quad (31)$$

Another mass-conservation relationship for the region between node N and node $N+1$ can be obtained from equation (2) as follows:

$$\Delta z\cdot\rho_s\cdot\frac{\partial\langle X_N\rangle}{\partial\tau}=-[(j_{wf})_{N+1}-(j_{wv}+j_{wb})_N]. \quad (32)$$

Combining equations (31) and (32), the moisture content at the node just above the evaporative plane may be obtained by solving the equation

$$\frac{-[(j_{wf})_{N+1}-(j_{wv}+j_{wb})_N]}{2\cdot\rho_s}=(-X_{N-1}-X_{\xi}+X_{FSP}+X_N)\cdot\frac{\partial\xi}{\partial\tau}+(\Delta z-\Delta z_{\xi})\cdot\left(\frac{\partial X_{N+1}}{\partial\tau}+\frac{\partial X_{\xi}}{\partial\tau}\right)+\Delta z_{\xi}\cdot\frac{\partial X_N}{\partial\tau} \quad (33)$$

where $(j_{wv}+j_{wv})_N$ is the sum of the vapour and bound-water fluxes at the node just above the evaporative plane, and $(j_{wf})_{N+1}$ is the liquid flux at the node just below the plane.

Solving equation (33) for the moisture content (X_N) ensures that the solution proceeds smoothly when the evaporative plane moves across a node point in a time step.

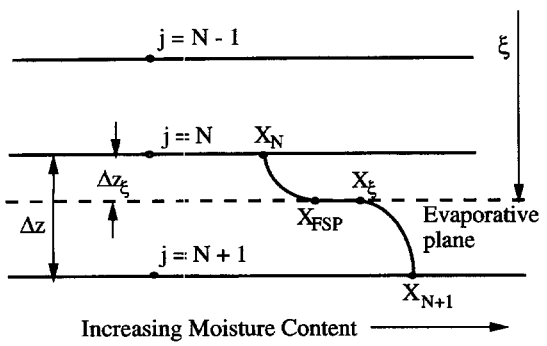

Fig. 2. The vicinity of the evaporative plane.

THE INITIAL CONDITIONS

For the green wood, the moisture content varies significantly between heartwood and sapwood. The heartwood is considerably drier in the natural state. Williams and Kininmonth [10] give the moisture content ranges for both heartwood and sapwood (40–50% for heartwood, 100–200% for sapwood), while Booker [11] indicates that much higher initial moisture contents are expected for younger trees (275–294% for the sapwood of a 7-year-old tree).

Because of the variability of initial moisture content with age and location, we regard the initial moisture content as a variable to be adjusted within these ranges so that the calculated length of the initial drying period agrees with that measured experimentally by Miller and Simpson [1]. In this work, only two initial moisture contents are used, one for heartwood and the other for sapwood. These two values have not been continually adjusted for each experiment.

The initial temperature of the wood has been assumed to be 20°C, which is close to typical ambient temperatures.

THE PHYSICAL PROPERTIES OF THE WOOD

The basic wood density varies with the distance from the pith and the height in the tree. The density of sapwood lies in the range 430–505 kg m^{-3}, while the range for heartwood is 338–404 kg m^{-3} [12]. For sapwood a value of 450 kg m^{-3} has been assumed, and the heartwood density has been assumed to be 400 kg m^{-3}.

Booker [11, 13] has measured the permeability of *P. radiata* to both gas and liquid flow, in both the green and dry state for sapwood and heartwood in both radial and tangential directions. His values span a considerable range, so both the permeability to gas flow and the permeability to liquid flow at saturation have been chosen so that the calculated temperature profiles for sapwood, heartwood and mixed wood agree with the experimental ones found by Miller and Simpson [1]. A comparison of the fitted values of the permeability with those measured by Booker [11, 13] provides a test of this approach.

The bound-water diffusion coefficient has also been chosen so that the calculated and measured temperature profiles agreed closely.

The specific heat capacity (C_P) and the thermal conductivity (λ) of moist wood have been predicted from the following correlations as functions of moisture content and dry-wood density (ρ_s) [2, 14]:

$$C_P = 4184 \cdot \frac{(X+0.324)}{1.0+X}$$

$$\lambda = \frac{\rho_s}{1000} \cdot (0.4+0.5X)+0.024.$$

These correlations relate to North American softwood species of broadly similar anatomy to *P. radiata.*

THE EXTERNAL CONDITIONS: THE TRANSFER-COEFFICIENT PROFILES IN THE STREAMWISE DIRECTION

Kho *et al.* [4] have shown that the local external mass- (or) heat-transfer coefficients vary from a maximum near the leading edge of a board to an asymptotic value at the trailing edge. This variation arises from the inevitable small gaps between adjacent, stacked boards [15]. An example of the extent of this variation is shown in Fig. 3 for a representative set of conditions, where the coefficients are interrelated through the identity

$$\beta = F \cdot \frac{m_v}{p_t} \tag{34}$$

where β is the mass-transfer coefficient based on partial-pressure differences, F is the mass-transfer coefficient based on the molar concentration differences [1], and p_t is the total pressure of the airstream.

If we take radiation into account, the heat-transfer coefficient can be related to the mass-transfer coefficient by the equation

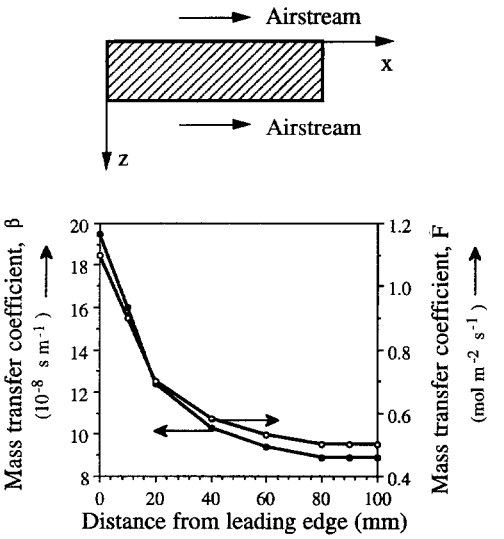

Fig. 3. The variation of local mass-transfer coefficients β and F with distance across the board in the airflow direction from the leading edge. Air velocity: 5 m s^{-1}. Boards: 100 mm × 50 mm. Sticker thickness (board gap): 25 mm.

$$h = 1.1 \cdot C_{PY} \cdot K_Y \tag{35}$$

where C_{PY} is the humid heat capacity of the gas, which is a function of the air humidity (Y_G) and the specific heat capacities of the gas (C_{PG}) and the vapour (C_{PV}):

$$C_{PY} = C_{PG} + C_{PV} \cdot Y_G. \tag{36}$$

In equation (35), K_Y is the mass-transfer coefficient based on mass concentration differences. It can be related to β by the expression [16]

$$K_Y = \beta \cdot \overline{p^G} \cdot \frac{m_G}{m_v} \tag{37}$$

where $\overline{p^G}$ is the average partial pressure of the air in the airstream, and m_G is the molar mass of air.

It follows that the profile of the local heat-transfer coefficients is similar to that of the mass-transfer coefficients.

RESULTS

In their experiments, Miller and Simpson [1] measured the dry-bulb temperature, the wet-bulb temperature, and the temperature at the centre and the surface of a board in both laboratory and commercial kilns. All the kiln charges were 100 mm × 50 mm undressed flat-sawn boards of green *P. radiata* consisting of sapwood, heartwood or mixed-wood stacks. The boards were dried at air velocities close to 5 m s^{-1} at a dry-bulb temperature of 120°C and a wet-bulb temperature of 70°C.

The experimental results are compared with the model predictions both to verify the simulation and to derive appropriate parameters. However, the model parameters have not been continually adjusted for each experiment, and the parameters have only been adjusted within credible limits. Biodiversity within

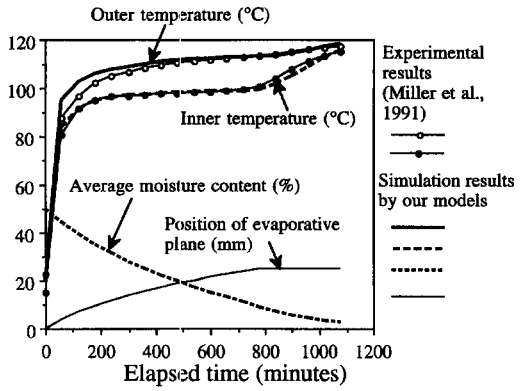

Fig. 4. Predicted temperature and moisture-content profiles and the predicted position of the evaporative plane as a function of time for 100 mm × 50 mm boards of heartwood, compared with the data of Miller and Simpson [1]. Initial moisture content, $X_o = 0.5$ kg kg^{-1}. Bound-water diffusion coefficient, $D_b = 8 \times 10^{-13}$ kg s m^{-3}. Vapour permeability, $K_G = 5 \times 10^{-16}$ m^2.

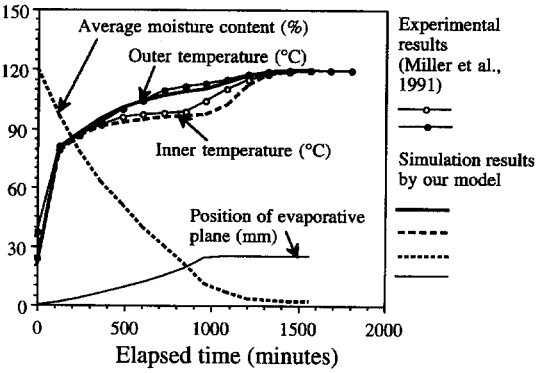

Fig. 6. Predicted temperature and moisture-content profiles and the predicted position of the evaporative plane as a function of time for 100 mm × 50 mm boards of mixed wood, compared with the data of Miller and Simpson [1]. Initial moisture content, $X_o = 1.2$ kg kg^{-1}. Bound-water diffusion coefficient, $D_b = 8 \times 10^{-13}$ kg s m^{-3}. Vapour permeability, $K_G = 7 \times 10^{-16}$ m^2. Liquid permeability, $K_l^s = 6 \times 10^{-16}$ m^2. Thickness of near-surface thin dry layer, $\xi_o = 0.45$ mm.

timber means that independent measurements of permeability, for example, vary widely within species, so our procedure of adjustment within measured limits is reasonable. Temperature profiles predicted by the model for heartwood, sapwood and mixed wood are given in Figs. 4–6, respectively, as well as the experimental data, and the fitted parameters are given below the figures. The predicted temperature profiles were produced by taking average values for the mass-transfer coefficient of 0.6 mol m^{-2} s^{-1} for comparison with the results for the small kiln where sapwood and heartwood were dried. A higher value of 0.7 mol m^{-2} s^{-1} has been chosen for the comparison with the data from the commercial kiln (used for the drying of mixed wood) in which somewhat higher velocities are suspected. These mass-transfer coefficients are consistent with the average values measured by Kho *et al.* [4].

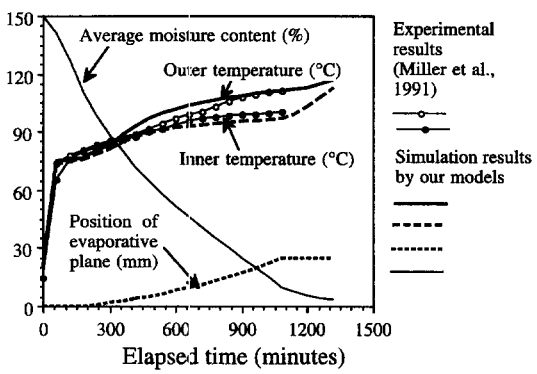

Fig. 5. Predicted temperature and moisture-content profiles and the predicted position of the evaporative plane as a function of time for 100 mm × 50 mm boards of sapwood, compared with the data of Miller and Simpson [1]. Initial moisture content, $X_o = 1.5$ kg kg^{-1}. Bound-water diffusion coefficient, $D_b = 8 \times 10^{-13}$ kg s m^{-3}. Vapour permeability, $K_G = 8 \times 10^{-16}$ m^2. Liquid permeability, $K_l^s = 6 \times 10^{-16}$ m^2. Thickness of near-surface thin dry layer, $\xi_o = 0.3$ mm.

The fitted parameters from this comparison and the variation of the heat- and mass-transfer rates with distance (Fig. 3) have been used to obtain the local temperature and moisture-content profiles along a board at different times from our drying model.

Figures 7 and 8 show these profiles for heartwood and sapwood, respectively, where the air is assumed to flow in one direction continuously under the same conditions as used by Miller and Simpson [1]. Both surface and centre temperatures in a board are given to show the variation of the temperature with depth into a board as well as distance along the board.

When the airflow is reversed periodically, the profiles of the heat- and mass-transfer coefficients along the boards will also be reversed. This reversal will change the development of the temperature and moisture-content profiles within the boards correspondingly. If we take the time interval for flow reversal as 4 h and use the instantaneous heat- and mass-transfer coefficient profiles at each flow reversal, we can obtain the local temperature and average moisture-content profiles for both heartwood (Fig. 9) and sapwood (Fig. 10) at different elapsed times.

The final profiles of the temperature and average moisture content shown in Figs. 7–10 are taken as those when the drying time is 24 h. This length of drying is recommended by Williams and Kininmonth [10] for *P. radiata* boards with a thickness of up to 50 mm in high-temperature drying. While schedules are now shorter, with 24 h being needed to accomplish the complete process including loading and unloading, the numerical calculations provide a relative guide to the changes in the final state with faster drying. The time interval between the instantaneous profiles is 4 h, which is the same as the period of the airflow rever-

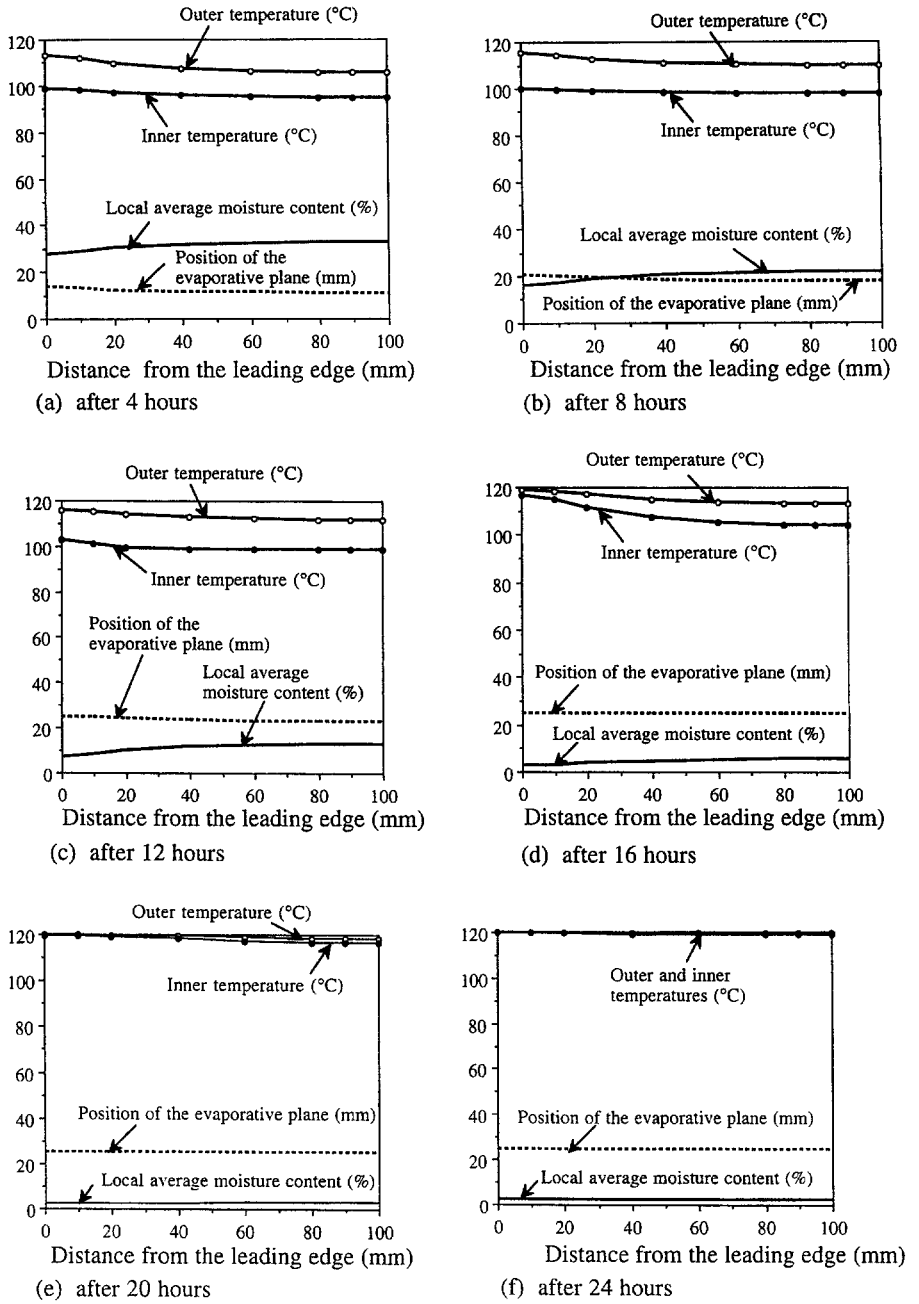

Fig. 7. The variations of the outer and inner temperatures, average moisture contents and the positions of the evaporative plane with distance along a board from the leading edge for heartwood (air flows in one direction).

sals. This time interval has been chosen for convenience in comparing the effect of airflow reversals on the profiles.

Figure 11 compares the temperature and moisture-content profiles inside a board of sapwood at the end of 8 and 24 h of drying for three cases where the airflow is reversed regularly at 4-h intervals, 8-h intervals, and where the airflow is only reversed once after 4 h of drying, respectively.

DISCUSSION

Comparison with experimental temperature profiles: heartwood

The temperature profiles shown in Fig. 4 for heartwood show that the outer and inner temperatures of the boards are significantly different throughout the drying process. This is consistent with our view of the drying process in heartwood, in which we assume that

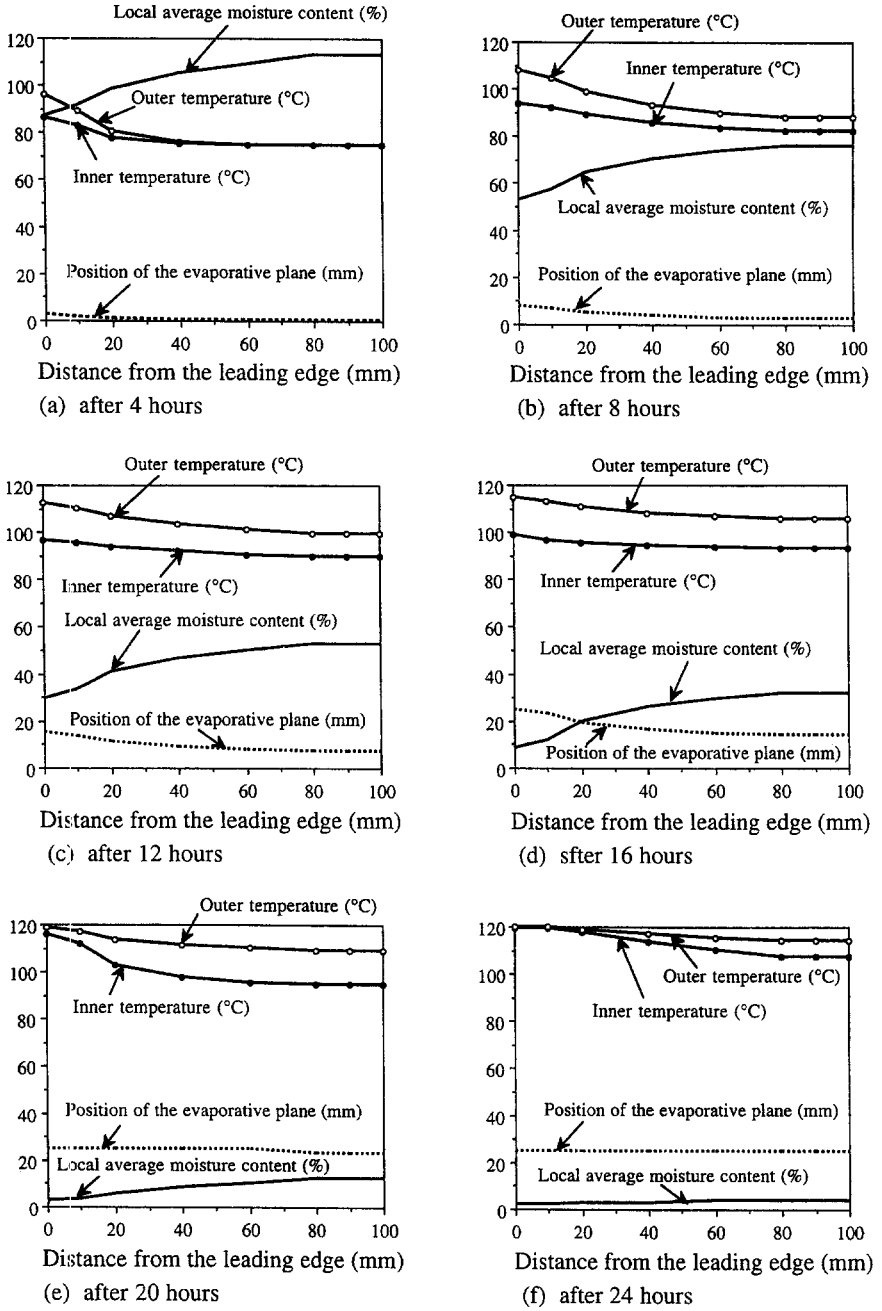

Fig. 8. The variations of the outer and inner temperatures, average moisture contents and the positions of the evaporative plane with distance along a board from the leading edge for sapwood (air flows in one direction).

the evaporative plane begins to recede from the start of drying due to the initially aspirated state of the pits. The inner temperature also remains near to the boiling point of water (100°C) for the first 800 min of drying, which is again consistent with the assumption in our model of an evaporative plane at the boiling point of water sweeping through the timber until the centre of the board is reached. Water is boiling from the tracheids, which are between 2 and 5 mm in length and 15–60 μm in diameter. The effect of these capillary sizes on raising the boiling point is small, as shown by the experimentally-measured temperatures staying close to 100°C during the initial drying period.

The differences between the calculated and measured temperature profiles are small and less than 6°C in all cases. In particular, the outer temperature is predicted to rise more rapidly than the measured temperature when the evaporative plane starts to recede into the board, and this may be due to the measured outer temperature actually being the temperature just

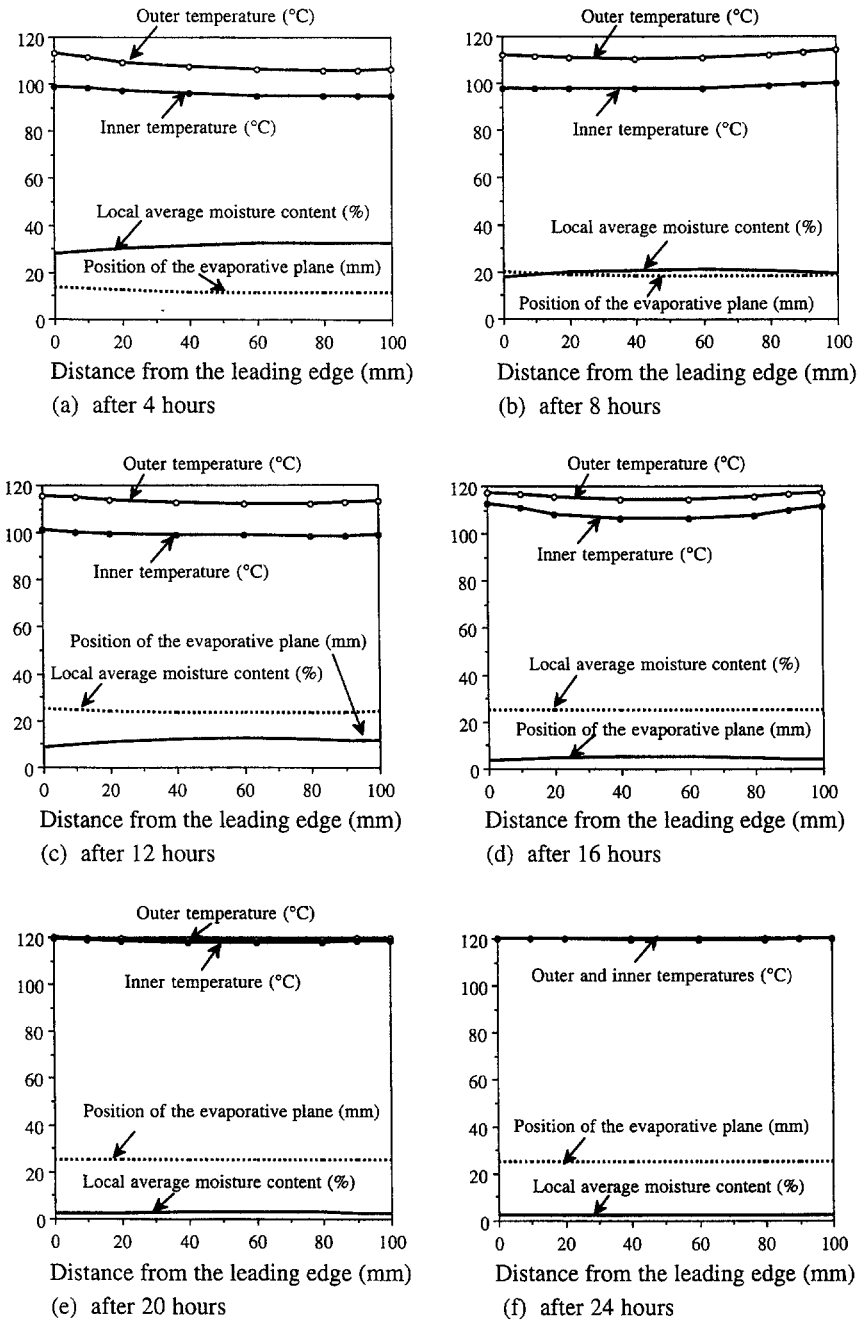

Fig. 9. The variations of the outer and inner temperatures, average moisture contents and the positions of the evaporative plane with distance along a board from the leading edge for heartwood (airflow is reversed every 4 h).

below the surface. This is likely when placing a thermocouple near the surface, since it may be necessary to push the thermocouple into the surface to get good thermal contact. Also, the measured inner temperature rises more sluggishly than that predicted during the first period of drying. This may be due to small errors in the estimate of the thermal conductivity of the timber, the vapour permeability or in experimental difficulties in trying to follow changing temperatures. The discrepancies are not large, however, giving some confidence in the predicted variation of the moisture content and the evaporative plane position with time.

Comparison with experimental temperature profiles: sapwood

In sapwood, the movement of liquid moisture must be considered since the initial moisture content is

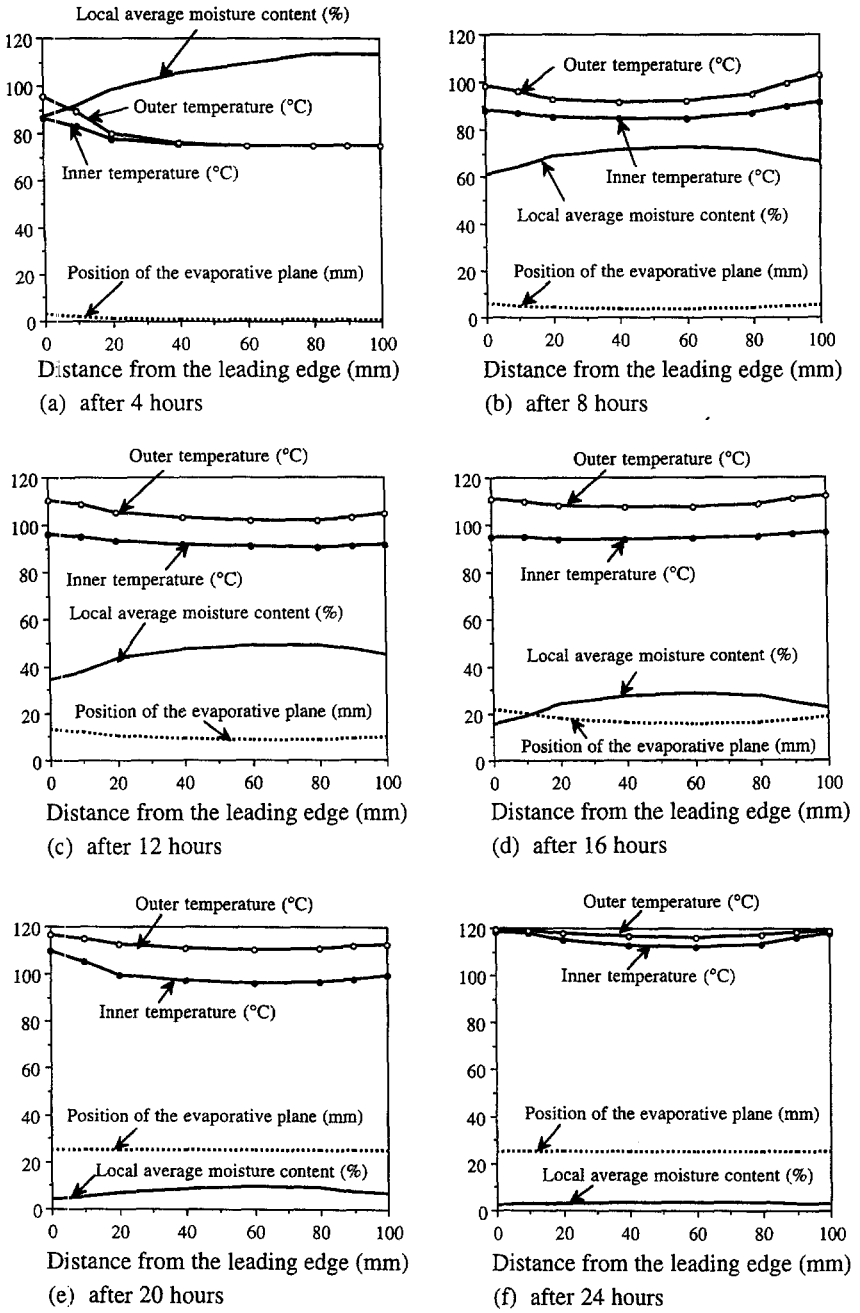

Fig. 10. The variations of the outer and inner temperatures, average moisture contents and the positions of the evaporative plane with distance along a board from the leading edge for sapwood (airflow is reversed every 4 h).

above the minimum moisture content for liquid water to be continuous throughout the timber, and the pits are not initially aspirated. This causes the evaporative plane to remain near the surface for a substantial period. In practice, staining of boards just under the surface has been observed in high-temperature drying [10], and this phenomenon may be the consequence of surface evaporation of this kind.

The inner temperature is initially very close to the outer one for the drying of sapwood (Fig. 5), and both temperatures rise gradually as drying proceeds. This suggests that the evaporative plane initially remains close to the surface, in agreement with the assumption made in our drying model of a thin dry layer a few tracheids wide. We believe that this behaviour of the evaporative plane is a feature of drying sapwood timber from softwoods. Thereafter, drying proceeds in a similar way to heartwood, with an increasing tem-

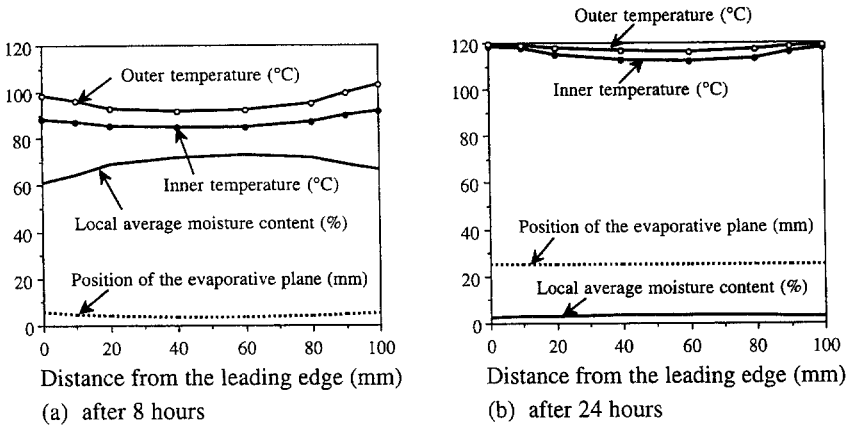

Airflow reversals every 4 hours

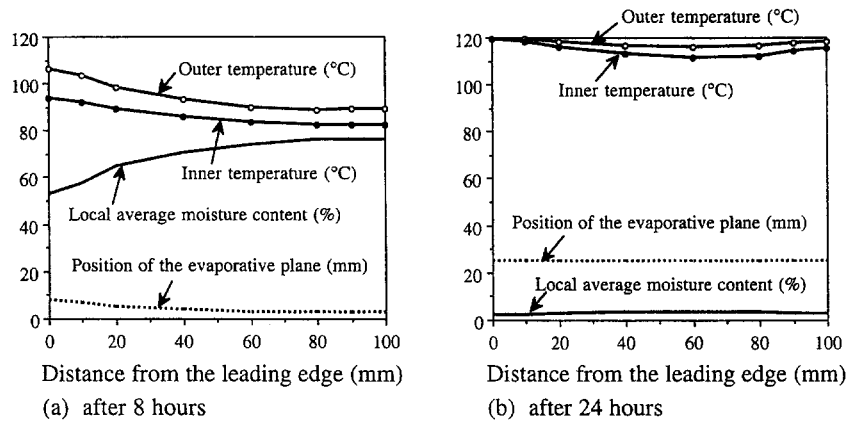

Airflow reversals every 8 hours

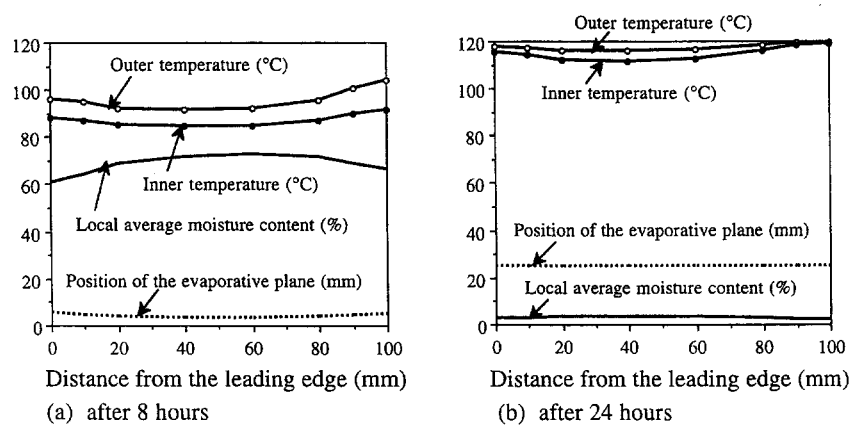

A single airflow reversal after 4 hours

Fig. 11. The variations of the outer and inner temperatures, average moisture contents and the positions of the evaporative plane with distance along the board from the leading edge for sapwood, using different policies for airflow reversals.

perature difference between the centre and the surface, suggesting that an evaporative plane is receding into the timber.

We have found that the best agreement between our fitted temperature profiles and those observed is obtained when we use a depth of the thin dry layer for the sapwood of 300 μm. This is about 10 times the mean tracheid width for softwood [17].

Comparison with experimental temperature profiles: mixed wood

Figure 6 shows that we can fit the temperature profiles for a load of unknown composition using reasonable values for the parameters in our drying model. For example, the fitted depth of the thin dry layer (450 μm) for mixed wood is greater than that for sapwood (300 μm), and this may be due to the averaging effect of having both sapwood (with a thin layer depth of 300 μm) and heartwood (with a much larger dried-out zone through which vapour flows) together.

Fitted permeabilities

The predicted drying behaviour is significantly affected by the assumed value of the permeability of the timber to vapour. If all other conditions are fixed, highly permeable timber offers less resistance to vapour transport and has a lower inner temperature. The fitted vapour permeabilities for heartwood (5×10^{-16} m^2), sapwood (8×10^{-16} m^2) and mixed wood (7×10^{-16} m^2) are very close to the value fitted by Stanish *et al.* [2] for Douglas fir (1×10^{-15} m^2). However, all these values are lower than the gas permeability of *P. radiata* sapwood and heartwood to air flow, as measured by Booker [13] ($32–138 \times 10^{-15}$ m^2 for dry sapwood, $8.8–78.6 \times 10^{-15}$ m^2 for dry heartwood). The fitted value for the liquid permeability of the sapwood and the mixed wood (600×10^{-18} m^2) falls in the range of the experimental values for green sapwood measured by Booker [11, 13] (radial direction: $18–168 \times 10^{-18}$ m^2; tangential direction: $169–774 \times 10^{-18}$ m^2). Booker [13] has found that dry sapwood is more permeable than dry heartwood to vapour flow, and our fitted values are in agreement with this observation. However, our predictions suggest that the difference between the permeabilities of sapwood and heartwood to vapour flow is not as significant as that measured by Booker [13].

The temperature and moisture-content profiles in the streamwise direction for unidirectional airflow

Heartwood. With unidirectional airflow (Fig. 7), the temperatures rise more swiftly, the evaporative plane recedes more deeply and the average moisture contents decrease more quickly for heartwood at positions near the leading edge than those at other places along the board in the airflow direction during the first period of drying. After 4 h of drying, the rate of rise of the temperature near the leading edge diminishes due to the loss of moisture at the surface, and the mass-transfer rate falls. Meanwhile, the differences in the average moisture contents and the receding velocity of the evaporative plane also decrease. When the evaporative plane at all points has reached the centre-line of the board, the moisture contents at the surface are nearly equal to the equilibrium moisture content (0.022 kg kg^{-1}), and the surface temperatures approach the dry-bulb temperature of the air. During the final period of drying, the heat- and mass-transfer rates at any point become much lower than those in the initial period of drying, and the differences in temperatures and average moisture contents along the boards become insignificant.

The largest temperature difference occurs on the surfaces between the leading and trailing edges, with a value of about 10°C after 2 h of drying, while after 14 h (when the evaporative plane at any point has reached the centre-line of the board) the surface temperature at the trailing edge is 5°C lower than that at the leading edge. However, at the end of 24 h drying, this temperature difference is predicted to be only 0.1°C.

The difference in average moisture contents between the leading and trailing edges is constant during the first period of drying, and remains at about 5% until the evaporative plane has reached the centre-line of the board at all positions. This moisture-content difference is mainly due to the variation in the depth of the evaporative plane along the board, because the moisture content in the dry zone (above the plane) is much lower than that in the wet zone (below it). Therefore this moisture-content variation is reduced during the second period of drying (after the evaporative plane at all positions has reached the centre-line of the board), and the moisture contents everywhere are estimated to be close to the equilibrium moisture content at the end of 24 h drying.

Sapwood. The variations in the profiles of the temperatures and the average moisture contents along the board for sapwood are significantly greater than those for the drying of heartwood (Fig. 9). During the initial period of drying, the evaporative plane near the leading edge remains close to the surface for a shorter time than at other positions, so the average moisture contents near the leading edge drop much more quickly than those elsewhere (27% lower than at the trailing edge after 4 h of drying). The largest surface temperature difference also occurs between the leading edge and the trailing edge, with a difference of 25°C after 6 h of drying. At the end of 24 h of drying, the moisture-content variation remains at about 2%, although at the leading edge the moisture content is close to the equilibrium moisture content.

The temperature and moisture-content profiles in the streamwise direction for airflow reversals

Heartwood. When the airflow is reversed at regular intervals, the differences in temperatures and moisture contents are greatly reduced. The degree of non-uniformity in both the temperature and moisture-content profiles is less for heartwood than for sapwood with unidirectional airflow. Airflow reversals may be expected to decrease the degree of non-uniformity in these profiles even more, thereby further reducing the number of drying defects.

After 16 h of drying with airflow reversals, the temperatures and moisture contents in heartwood (Fig. 10) are already relatively uniform (within 5°C and 2% respectively). No significant benefit can be obtained by further reversals of the airflow.

Sapwood. For sapwood, the most non-uniform profiles of the temperatures and average moisture contents occur after 4–8 h of drying (Fig. 11). Just before the airflow is reversed after 4 h of drying, the surface temperature at the leading edge is 20°C higher and the moisture content there is 23% lower than the corresponding values near the trailing edge. However, after the airflow has been reversed once, these differences fall to 10°C for the temperatures and 10% for the average moisture contents. At this time (after 8 h of drying), the temperatures are similar at the positions near the ends of the board and higher than those in the middle area of the board. Further airflow reversals should give more uniform temperature and moisture-content profiles regardless of whether the evaporative plane has reached the centre-line of the board at all distances from the leading edge or not. The lower temperatures and higher moisture contents in the middle of the board are due to the lower average heat- and mass-transfer rates outside the board, even though the airflow has been reversed several times.

Superimposed on the variations of moisture content and temperature over each board are those board-to-board variations caused by the progressive humidification and cooling of the air as it passes through the timber stack in the kiln. These variations reduce the driving force and thus the differences in temperature and moisture content across each board progressively in the airflow direction. Our calculations, therefore, apply to short stacks when the within-board variations are the greatest. Kilnwide variations in local average moisture contents and drying rates of the boards are investigated by Keey and Ashworth [19] for low-temperature drying of *P. radiata*. As found in our analysis of the variations over a single board, airflow reversals reduce variability of moisture content, but not many reversals are needed.

CONCLUSIONS

We are able to predict the variation of the surface and centre temperature with time in the high-temperature drying of individual *P. radiata* boards. It is postulated for heartwood that an evaporative plane at the moisture boiling point sweeps through the timber. In the case of the much wetter sapwood board, we assume that at first the liquid flows maintain an evaporative plane just below the surface until the moisture in no longer funicular. Thereafter, drying proceeds in a similar way to heartwood. Once the timber is below the fibre saturation point, cell-wall diffusion controls. These assumptions are in accordance with models for pit aspiration [13]. The fitted parameters in our drying model are measurable and generally fall within the range of measured values, except for our fitted value for vapour permeability which is much lower than measured values. The good agreement between the measured and observed temperature profiles gives some confidence that the variations in moisture content and position of the evaporative plane have also been simulated closely.

Using the profiles of the measured mass-transfer coefficients from Kho *et al.* [4], we can predict the local temperatures and moisture contents. When air flows in one direction only, the temperatures are higher and the moisture contents are lower at the leading edge than in other positions due to the variation of heat- and mass-transfer rates along the boards. These differences can be reduced by airflow reversals, and this should reduce the number of drying defects. It is recommended that airflow reversals can be halted or the time interval can be lengthened after the airflow has been reversed 4 times (with 4-h intervals between airflow reversals) for heartwood drying. This recommendation also applies to the drying of sapwood, provided that a value of 3°C for the final temperature variation and a value of 2% for the final moisture-content difference are acceptable. The predictions of our model also suggest that, for the drying of sapwood boards, an 8-h interval between airflow reversals (every working shift), or a single airflow reversal after 4 h of drying, is a minimum requirement for the moisture contents across the width of the boards to vary by less than 20% at any time during drying.

Acknowledgements—The authors would like to thank Mr W. R. Miller and Mr I. G. Simpson of the Forest Research Institute, Rotorua, New Zealand, for their assistance with the experimental work, and the Ministry of Forestry, New Zealand, for partial financial assistance. We also thank the State Education Commission, People's Republic of China, for financially supporting one of us (P.S.S.), and we acknowledge the award of a scholarship from the New Zealand Ministry for External Relations and Trade to enable the work to be continued. The authors are grateful for helpful discussions with Dr J. C. F. Walker of the School of Forestry, University of Canterbury, in carrying out this work.

REFERENCES

1. W. R. Miller and I. G. Simpson, Temperature data files, Private communication, New Zealand Forest Research Institute, Rotorua (1991).
2. M. A. Stanish, G. S. Schajer and F. Kayihan, A mathematical model of drying for hygroscopic porous media, *A.I.Ch.E. Jl* **32**(8), 1301–1311 (1986).
3. P. Perré, J. P. Fohr and G. Arnaud, A model of drying applied to softwood : the effect of gaseous pressure above the boiling point, *Proceedings of the Sixth International Drying Symposium IDS'* 88, Versailles, pp. 279–286 (1988).
4. P. C. S. Kho, R. B. Keey and J. C. F. Walker, Effect of minor board irregularities and air flows on the drying rate of softwood timber board in kilns, *Proceedings of the Third IUFRO International Wood Drying Symposium*, Seattle, pp. 150–157. International Union of Forestry Research Organizations (1989).
5. R. E. Booker, Hypothesis to explain the characteristic appearance of aspirated pits, *Proceedings of the 2nd Pacific Region Wood Anatomy Conference*. Forest Products Research and Development Institute, Laguna (1989).
6. W. T. Simpson and H. N. Rosen, Equilibrium moisture content of wood at high temperature, *Wood and Fibre* **13**(3), 150–158 (1981).

7. G. A. Spolek and O. A. Plumb, Capillary pressure in softwood, *Wood Sci. Technol.* **15,** 189–199 (1981).
8. S. Patankar, *Numerical Heat Transfer and Fluid Flow*, p. 58. Hemisphere, New York (1980).
9. W. H. Press, B. P. Flannery, S. A. Teukolsky and W. T. Vetterling, *Numerical Recipes. The Art of Scientific Computing*, p. 40. Cambridge University Press, Cambridge, MA (1986).
10. D. H. Williams and J. A. Kininmonth, High temperature kiln drying of radiata pine sawn timber, New Zealand Forest Service, Forest Research Institute Bulletin No. 73, Rotorua (unpublished) (1984).
11. R. E. Booker, A comparison of the radial, tangential and axial permeabilities of radiata pine, New Zealand Forest Service, Forest Research Institute, Timber Drying Report No. 39, Rotorua (unpublished) (1979).
12. D. J. Cown, D. L. McConchie and G. D. Young, Radiata Pine Wood Properties Survey, New Zealand Forest Service, Forest Research Institute Bulletin No. 50 (revised), Rotorua (unpublished) (1991).
13. R. E. Booker, Changes in transverse wood permeability during the drying of *Dacrydium cupressinum* and *Pinus radiata*, *N.Z.J. Forestry Sci.* **20**(2), 231–244 (1990).
14. F. Kayihan, Simulation of heat and mass transfer with local three-phase equilibria in wood drying, *Proceedings of the Third International Drying Symposium*, Birmingham, Vol. 1, pp. 123–134 (1982).
15. T. A. G. Langrish, P. C. S. Kho, R. B. Keey and J. C. F. Walker, Experimental measurement and numerical simulation of local mass-transfer coefficients in timber kilns, *Drying Technol.* **10**(3), 753–781 (1992).
16. R. E. Treybal, *Mass Transfer Operations* (3rd Edn), p. 49. McGraw-Hill, New York (1980).
17. J. F. Siau, *Transport Processes in Wood*, p. 44. Springer-Verlag, Berlin (1984).
18. W. R. Miller, Private communication (1992).
19. R. B. Keey and J. C. Ashworth, The kiln seasoning of softwood timber boards, *Chem. Engr* **347/8,** 593–602, 607 (1979).